Threading the needle: constraining the stellar content and dynamics of the Galactic Centre with hypervelocity stars

Verberne, S.

1 Introduction

The omnipresent and almost unchanging night sky has been has been a source of fascination for much of human history. Some of the earliest records of astronomical observations originate from Babylonia in ancient Mesopotamia—the very birthplace of human civilization—dating back some 4000 years (Steele 2021). Astoundingly, modern astronomy can be traced back through a continuous tradition to these early observations (Evans & Friedlander 2025). The practical use of astronomy for, in particular, time-keeping and navigation have allowed it to be remain relevant during much of this time. Of course, our understanding of the night sky has transformed almost beyond recognition over the ages.

Modern astronomy perhaps started with the first astronomical observations using a telescope published in Galilei (1610). Although revolutionary at its time, observational techniques have come a long way since this first study. Through incremental improvement in our telescopes and understanding of physics we are closer now than ever to understanding our place in the Universe. This is not to say that all the mysteries of the Universe will be solved within a few years. We have discovered many types of objects and phenomena that were simply not known even one hundred years ago, and continue to discover new ones. Sometimes a mysterious phenomenon is observed that eludes a rigorous theoretical explanation for decades, while other times a theoretical prediction is put forward, only to be observed much later. This thesis deals with one such class of object, known as hypervelocity stars (HVSs), which can travel at millions of kilometres per hour through our Galaxy, which we show schematically in Fig. 1.1.

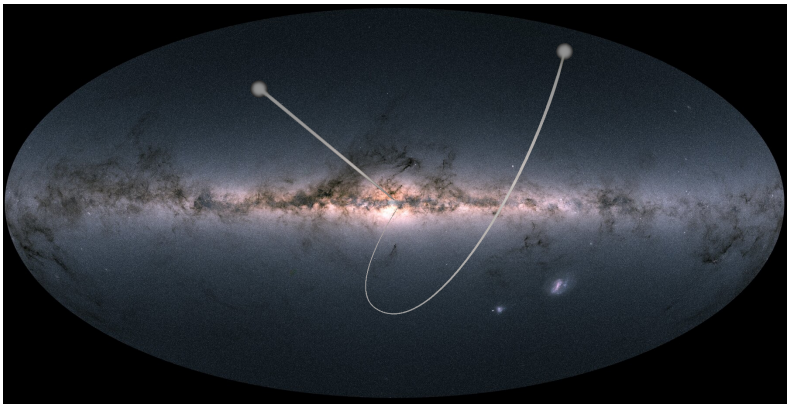

Figure 1.1: Schematic illustration of HVSs which travel through the Galaxy with extreme velocities. *Image credit: ESA + Gaia DPAC (modified).*

Already in 1988 the theoretical prediction was made that some stars should exist that are ejected from our Galaxy at extreme velocities through the interaction with a massive black hole, but it took until 2005 for the first such star to be discovered. To this day we know precious few HVSs despite significant efforts to discover more of them. This is in large part due to their extreme rarity; only about one in one hundred million stars in our Galaxy is expected to be an HVS (Verberne et al. 2024a).

HVSs are the thread throughout this thesis. We will discuss and apply various methods, combining observations and simulations, to search for these stars. Furthermore, we will discuss in depth how the limited observational knowledge of HVSs can nonetheless be used to place meaningful constraints not only on the properties of HVSs, but on the Galaxy itself.

In this introduction we will first discuss the major stellar components of the Galaxy in Section 1.1. In Section 1.2, we discuss HVSs, including how the field progressed from the first theoretical prediction to the present, the theoretical model for how these stars are ejected, a number of the science cases for the study of HVSs, and alternative mechanisms through which such stars might be produced. Section 1.3 describes the two most important astronomical surveys that are used in this thesis and covers the main instrumentation and data products. In Section 1.4 we cover future prospects of the field of HVSs. Finally, Section 1.5 provides an overview of the main scientific chapters of this thesis.

1.1 Structure and dynamics of the Milky Way

Advances over the past century have allowed us to gain a detailed understanding of our host galaxy: the Milky Way. This has allowed us to subdivide the Galaxy in a number of main components: the stellar halo, disc(s), bulge, bar, and Galactic Centre (GC). Fig. 1.2 shows a schematic overview of these components and their geometry. In this section, we will go over the main components of the Galaxy from the outside in.

1.1.1 Stellar halo

The classical view of the stellar halo is that it is a roughly spherical and isotropically distributed population of old, metal-poor stars that surrounds the Galaxy. We now know that is is not an accurate view of the stellar halo.

The current paradigm for galaxy formation is that galaxies grow through hierarchical mergers with satellites (Press & Schechter 1974; White & Rees 1978). These past mergers have build up a cloud of stars around the Galaxy at distances up to 100 kpc, forming the stellar halo (for recent reviews, see Helmi 2020; Deason & Belokurov 2024). The stars in the stellar halo are predominantly old and metal-poor and the atmospheres of these stars

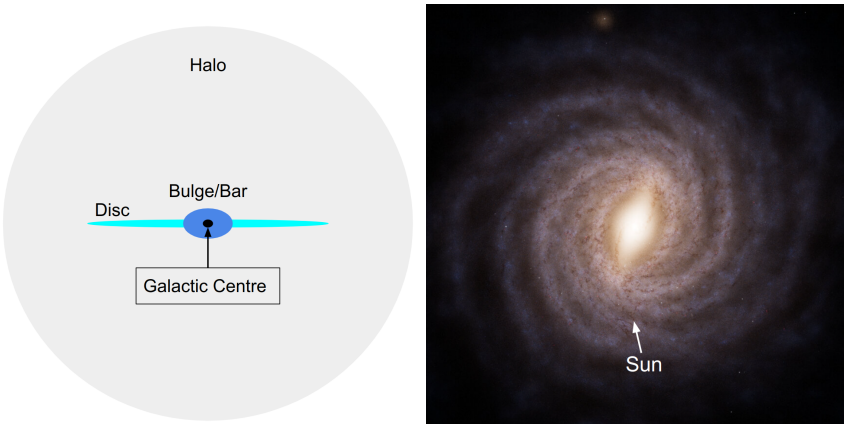

Figure 1.2: Left: side-on schematic overview of the Milky Way Galaxy (not to scale). Some of the major components of the Galaxy are labelled. Right: artist impression of the Milky Way from a top-down view (*adapted from image by: ESA/Gaia/DPAC, Stefan Payne-Wardenaar*).

contain crucial information on their satellite galaxy birth environments. These properties allow us to study the high-redshift progenitor satellites and make comparisons to observations of the distant Universe (e.g. Helmi 2020).

The stellar halo near the Sun is dominated by a single merger, which happened about 10 billion years ago, the remnant of which is known as the *Gaia* Sausage/Enceladus (GSE; Belokurov et al. 2018; Helmi et al. 2018; Haywood et al. 2018). The stars that are part of GSE are characterised by their highly elliptical orbits through the Galaxy and their relatively high metallicity for the stellar halo (mean [Fe/H] ~ -1.2; Feuillet et al. 2021). GSE is considered the last major merger of the Galaxy and has helped shape many of the current properties of the Galaxy (Naidu et al. 2021). The peculiar name of this structure is traced back to the two groups who discovered it (Belokurov et al. 2018; Helmi et al. 2018) and the shape it takes in Galactic radial against circular motion, as shown in Fig. 1.3.

The stellar halo is also marked by stars that orbit the Galaxy in coherent thin strings, known as stellar streams (for a recent review, see Bonaca & Price-Whelan 2025). These streams are formed by low mass dwarf galaxies and star clusters that merge with the Galaxy. The tidal force from the Galaxy causes some stars in the satellite to have slightly shorter or longer orbital periods. The effect is that stars escape from the satellite through the leading and trailing tidal tails (Binney & Tremaine 2008).

Furthermore, the stellar halo contains two notable dwarf galaxies called the Large and Small Magellanic clouds (LMC; SMC), which are the most

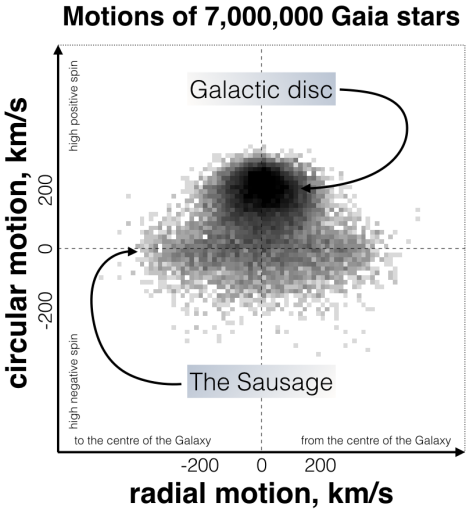

Figure 1.3: The GSE shown in Galactic radial against circular velocity. The GSE has an elongated 'sausage' shape in this space. *Image credit: V. Belokurov (Cambridge, UK and CCA, New York, US) and Gaia/ESA.*

massive Milky Way satellites. The LMC and SMC are visible by eye from the southern hemisphere and are located at about 50 and 62 kpc from the Sun respectively (e.g. Pietrzyński et al. 2019; Graczyk et al. 2020). Fig. 1.4 shows a picture of the LMC and SMC taken from Paranal, Chile. Especially the LMC is important for dynamics in the stellar halo due to its high mass. The enclosed mass of the LMC within 32.8 kpc is $\sim 7 \times 10^{10}$ $M_\odot$, while the enclosed mass of the Milky Way within 32.4 kpc is $(2.85 \pm 0.1) \times 10^{11}$ $M_\odot$ (Erkal et al. 2019; Vasiliev et al. 2020; Reino et al. 2021; Shipp et al. 2021; Koposov et al. 2023). Trajectories of stars in the stellar halo can therefore be significantly affected by the LMC and the reflex motion of the Milky Way in response to the LMC has already been measured along with the LMC induced wake (Garavito-Camargo et al. 2019; Erkal et al. 2021; Petersen & Peñarrubia 2021; Conroy et al. 2021; Vasiliev et al. 2021; Cavieres et al. 2025).

1.1.2 Stellar discs

Embedded in the stellar halo are two aligned discs of stars, which also contain our solar system: the thin and thick discs. The thin disc contains most of the stars in our Galaxy and contains younger stars than the thick disc. The naming of these two discs stems from their scale heights; the thin disc having a significantly smaller scale height compared to the thick disc.

Figure 1.4: The Magellanic clouds seen from Paranal, Chile. The LMC and SMC are the bright clouds in the middle and top of the frame respectively. *Image credit: ESO/J. Colosimo.*

The existence of the thick disc was already suggested in Gilmore & Reid (1983), but has been debated till recently (e.g. Rix & Bovy 2013). The scale heights of the thin and thick disc are about 300 and 1000 pc respectively (e.g. Jurić et al. 2008). The Sun is part of the thin disc and is located about 20.8 pc above the Galactic mid-plane (Bennett & Bovy 2019).

In addition to the scale height, the thin and thick discs are also distinct in their abundance patterns. In particular, the thick disc is enhanced in [α/Fe] compared to the thin disc for a given [Fe/H]. [α/Fe] indicates the abundance of α elements with respect to iron. This ratio is highly informative on the origin of stars, because α-element enrichment mainly occurs through type II supernovae (e.g. Gilmore & Wyse 1991), which are the endpoints for massive stars, while iron is formed by all supernova.

An explanation of the thick disc that has been suggested is that it contains stars from a protodisc, which was dynamically heated by the last major merger of the Galaxy that resulted in the previously discussed GSE (Belokurov et al. 2018; Xiang & Rix 2022; Chandra et al. 2024).

The most dramatic substructures of the Galactic disc are the spiral arms (see Fig. 1.2), the formation of which are still a matter of debate (Lin & Shu 1964; Toomre 1964; Wada et al. 2011; Shu 2016; Shen & Zheng 2020; Castro-Ginard et al. 2021). Furthermore, determining the spiral structure of the Milky Way is challenging, because we observe the Galaxy from within

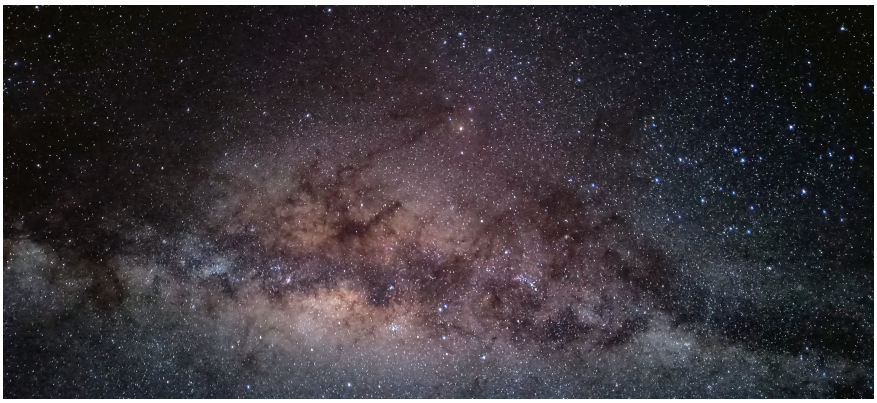

Figure 1.5: Picture including the central region of the Milky Way as seen from La Silla, Chile. *Picture by Sill Verberne.*

(e.g. Hou et al. 2009; Hou & Han 2014). It is believed that the Galaxy has four major spiral arms and that the Sun is located in the Local Arm, which is a subsidiary that extends between two of the major spiral arms (e.g. Shen & Zheng 2020; Poggio et al. 2021).

1.1.3 Bar and bulge

Closer to the centre of our Galaxy, the spiral arms make way for the bar and bulge (see Fig. 1.2). In the central few kiloparsecs of the Galaxy, we find a boxy/peanut bulge with an X-shape that forms an out-of-plane structure (Weiland et al. 1994; Dwek et al. 1995; Binney et al. 1997; McWilliam & Zoccali 2010; Wegg & Gerhard 2013; Wegg et al. 2015; Ness & Lang 2016; Barbuy et al. 2018). This bulge component is likely related to the bar. In fact, most of the stars in the bulge might belong to the central bar, which we view nearly end-on (Shen & Zheng 2020). The bar consists of stars on elliptical orbits and rotates with a pattern speed of $\Omega_{\rm bar} = 38.1^{+2.6}_{-2.0}$ km s^{-1} (Gaia Collaboration et al. 2023b). The bar and the spiral arms are the two most notable non-axisymmetric stellar components of the Milky Way.

1.1.4 Galactic Centre

At the very centre of our Galaxy we find a complex region where many stellar populations overlap. Fig. 1.5 shows an image of the GC region and surrounding area taken from Chile with a phone camera. At optical wavelengths such as shown in the image, the Galactic Centre (GC) itself is hidden behind a strong extinction layer ($A_{\rm V} \sim 50$; Fritz et al. 2011). For this reason,

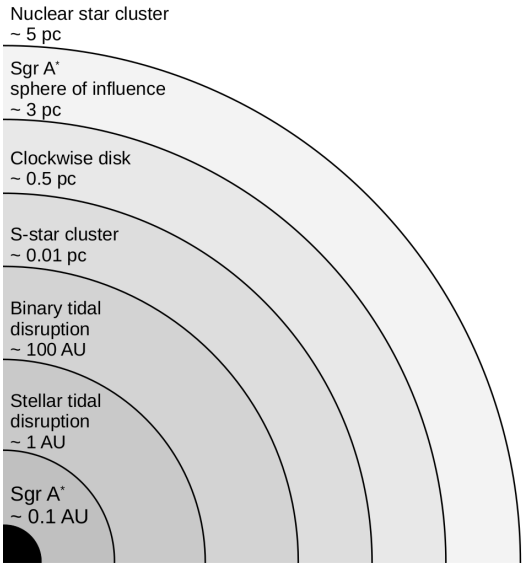

Figure 1.6: Schematic view of the different structures in the central parsecs and their distance from Sgr A*.

the GC has often been studied at lower frequencies (e.g. Ghez et al. 1998; Genzel et al. 2003; Event Horizon Telescope Collaboration et al. 2022a) or X-rays (e.g. Baganoff et al. 2001; Degenaar & Wijnands 2009; Hailey et al. 2018) where the extinction is lower. To provide an understanding of the physical scales at the GC, we include Fig. 1.6. At the centre of the Galaxy sits the super massive black hole Sagittarius A* (Sgr A*), first discovered at radio wavelengths in Balick & Brown (1974). Sgr A* is located about 8.3 kpc from the Sun and has a mass of about 4.3×10^6 $M_\odot$ (Eisenhauer et al. 2005; Ghez et al. 2008; Schödel et al. 2009; Gillessen et al. 2009; Boehle et al. 2016; Gillessen et al. 2017; Do et al. 2019; GRAVITY Collaboration et al. 2019, 2022b), which means that the Schwarzschild radius $R_s = 2GM/c^2$ is close to 0.1 AU. Recent advances in very-long baseline interferometry have made it possible to obtain observations on scales similar to the Schwarzschild radius, resulting in the first publication of an image of Sgr A* (Event Horizon Telescope Collaboration et al. 2022a,b,c,d,e).

At about 10 times the Schwarzschild radius is the tidal disruption radius, where a star is torn apart by the tidal force from the black hole in a transient event known as a tidal disruption event (TDE; Hills 1975; Rees 1988; Rossi et al. 2021; Gezari 2021). Further out at roughly 100 AU is the radius at which binary stars are separated by the tidal force of Sgr A*, discussed in detail in Section 1.2.2.

The closest population of stars to Sgr A* is known as the S-star clus-

ter, which is a cluster of stars on isotropically distributed orbits with high eccentricities and semi-major axes up to ~ 0.04 pc (Genzel et al. 2010). The cluster is mainly composed of main-sequence B-type stars, but some evolved stars have also been found in the S-star cluster (e.g. Gillessen et al. 2017). It is unclear how these stars formed, since the strong tidal force so close to Sgr A* should inhibit star formation (Ghez et al. 2003). This lack of understanding on the origin of this cluster persists despite the fact that the S-star cluster has been intensely studied over the past decades (Eckart & Genzel 1996; Ghez et al. 1998). The main reason that the S-star cluster has been studied so much is its proximity to Sgr A*. Because these stars are so close to Sgr A*, their orbital periods are on a timescale that can now be resolved. The star S2 has been of particular importance for our understanding of the GC and Sgr A*, since it is a bright star ($m_{\rm K} = 14$) on an orbit of ~ 16 years (Habibi et al. 2017a). Only a single star has been detected on a shorter orbit (S55; ~ 13 years), but since that star is much fainter at $m_{\rm k} = 17.5$ it is also less constraining due to the difficulty of observing it. The monitoring of orbits of individual stars in the S-star cluster is how researchers have been able to determine the mass and distance to Sgr A* with an unprecedented precision. In recent years, tests of general relativity have even become possible based on observations of the S-star cluster, since Schwarzschild precession has now been measured for multiple stars (GRAVITY Collaboration et al. 2020; Gravity Collaboration et al. 2024). As an excellent example of how important the S-star cluster has been for astronomy, half of the Nobel Prize in Physics 2020 was awarded to Reinhard Genzel and Andrea Ghez 'for the discovery of a supermassive compact object at the centre of our galaxy'. Observations of the S-star cluster were what made this discovery possible.

At ~ 0.04 pc a transition occurs between the S-star cluster and at least one (warped) disc of massive stars (e.g. Levin & Beloborodov 2003; Paumard et al. 2006; Bartko et al. 2009; von Fellenberg et al. 2022). This so called clockwise disc (CWD) contains many O/WR stars out to ~ 0.5 pc, while no O/WR stars are detected within the S-star cluster. In addition, stars in the CWD travel on relatively low eccentricity orbits in comparison with the S-star cluster. The CWD is one of the only regions in the Galaxy where a top-heavy initial mass function (IMF) has been suggested (Paumard et al. 2006; Bartko et al. 2009; Lu et al. 2013; Gallego-Cano et al. 2024). The most likely origin of the CWD is through a burst of star formation in a gaseous disc (Levin & Beloborodov 2003; Paumard et al. 2006; Levin 2007). It is still uncertain if and how the CWD and S-star cluster are related.

Encompassing Sgr A*, the S-star cluster, and the CWD is the nuclear star cluster (NSC), with a half-light radius of about 5 pc (Schödel et al. 2014). The NSC is a much older population of stars compared to the S-star cluster and CWD, with most of the stellar content having formed billions of years ago (e.g. Pfuhl et al. 2011; Chen et al. 2023). The NSC is the densest

stellar cluster in the Galaxy with on the order of 10^6 stars per cubic parsec (e.g. Schödel et al. 2007). The Milky Way is not the only galaxy with a NSC, in fact they are observed at the centres of most galaxies (for a recent review, see Neumayer et al. 2020).

1.2 Hypervelocity stars

Now that we have discussed the general structure of the Milky Way, we will discuss the main subject of this thesis: HVSs (for review, see Brown 2015). We will start by going over some of the original discoveries, before going over the basic concepts of how these objects are formed.

1.2.1 From the first prediction to the present

Hills (1988) first predicted that if a stellar binary would approach a massive black hole (MBH) to within the tidal radius, where the tidal force from the MBH overcomes the self-gravity of the binary, one star would get captured into a tight elliptical orbit while the companion would get ejected at velocities potentially in excess of the escape velocity from the Galaxy. Hills dubbed the ejected stars HVSs, while the ejection mechanism has since been referred to as the Hills mechanism. When this prediction was first published, there was still active debate about the mere existence of MBHs. In fact, Hills (1988) suggested that the discovery of an HVS would provide near definitive evidence for a MBH. In Hills (1991), the original work was expanded upon with additional simulations exploring the parameter space.

It was not until the early 2000s that the subject started to gain more attention, for instance in Gould & Quillen (2003), who suggested that the star S2 might have been put onto its close orbit around Sgr A* by a tidal binary separation. The ejection of stars from the GC was revisited in Yu & Tremaine (2003), where the authors discussed three mechanisms through which stars might be ejected from the GC: close encounters of single stars, binary disruptions by a MBH (Hills mechanism), and the ejection of a single star by a binary black hole (BBH). The real breakthrough for the subject, however, came with the discovery of the first HVS in Brown et al. (2005) called HVS1. This serendipitous discovery was soon followed up by more HVS discoveries (Hirsch et al. 2005; Edelmann et al. 2005; Brown et al. 2006a,b) and marked the start of a wave of renewed interest in the subject.

About a decade later, there were a few tens of HVSs found in the literature, most notably by the MMT survey (Brown et al. 2009, 2012, 2014), which targeted blue stars in the stellar halo. These HVS discoveries tended to be distant ($\gtrsim 50$ kpc) main-sequence stars with Galactocentric velocities up to $\sim 700\ \mathrm{km\,s^{-1}}$. A side effect of the large distances to these stars is

the difficulty of constraining their past trajectories. Nonetheless, in further studies, it was found that at least some of the HVSs in fact cannot originate in the GC (e.g. Gualandris & Portegies Zwart 2007; Brown et al. 2018; Boubert et al. 2018) and alternative ejection origins proved difficult to rule out in general (see Section 1.2.3). This highlighted a potential issue for the science exploitation of these objects, because many of the science cases specifically rely on a GC ejection origin (see Section 1.2.4). The first, and currently only, unambiguous discovery of an HVS originating in the GC was presented in Koposov et al. (2020): a $\sim 1700\ \mathrm{km\,s^{-1}}$ star that is relatively nearby (~ 9 kpc) and whose trajectory traces back to the GC called S5-HVS1. The combination of extreme velocity—much higher than previously discovered HVSs—and the relative proximity were what truly set this star apart from the previous discoveries. Interestingly, HVS1 and S5-HVS1, arguably the two most important stars in the field currently known, were both serendipitously discovered.

It should be noted at this point that the term HVS has not been consistently used in the literature. Brown (2015) define an HVS to be characterised by an MBH ejection origin and an unbound velocity. A complicating factor here is that in reality it is often uncertain if a star is unbound because of uncertainties in the Galactic potential, the stellar velocity, and its distance from the Sun. Additionally, alternative mechanisms exist that can accelerate stars to near, or in excess of, the Galactic escape velocity (see Section 1.2.3). Throughout this thesis, we define HVSs to be stars ejected from the vicinity of Sgr A*.

1.2.2 Hills mechanism

Having discussed some of the most important advances in the field of HVSs, we will now go over some of the theoretical aspects of the Hills mechanism. First we discuss the general principle through which a gravitational interaction near an MBH can cause a star to gain significant energy, where we follow the argumentation from Yu & Tremaine (2003). Suppose we have a star with specific energy $E = \frac{1}{2}v^2 + \Phi(r)$, where v is the velocity and $\Phi(r)$ is the specific potential energy. Close to the MBH $|\Phi(r)| \gg |E|$, which means that the star will travel approximately at the free-fall velocity. If, at this time, the star experiences a velocity perturbation $\delta v \ll v$, the specific energy of the star will change by $\delta E = \frac{1}{2}(v + \delta v)^2 - \frac{1}{2}v^2 \simeq v\delta v$. For a relatively modest increase in velocity δv, δE can become much larger than $|E|$, which means that the star is ejected. In the Hills mechanism, the velocity perturbation is caused by the tidal separation of a stellar binary. As mentioned before, a stellar binary is separated by an MBH when the tidal force of the MBH exceeds the self-gravity of the binary. The radius at which

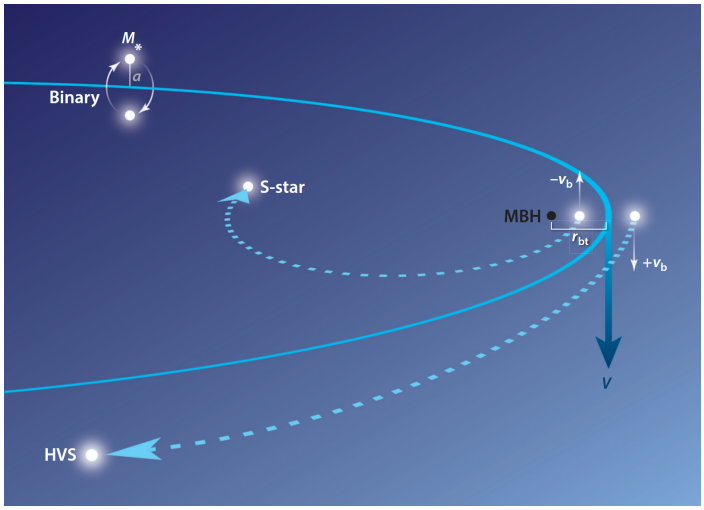

Figure 1.7: Schematic illustration of the Hills mechanism in which a stellar binary is separated by the tidal force from an MBH. *Image from Brown (2015).*

this occurs is the tidal separation radius

$$r_{\rm t} = a_{\rm b} \left(\frac{M_{\rm MBH}}{m_{\rm b}} \right)^{1/3}, \tag{1.1}$$

where $a_{\rm b}$ is the semi-major axis of the progenitor binary, $M_{\rm MBH}$ the mass of the MBH, and $m_{\rm b}$ the mass of the stellar binary. Note that in reality a binary can be disrupted at larger radii and survive at smaller radii (Sersante et al. 2025). A schematic illustration of this process is shown in Fig. 1.7.

If the progenitor binary is on a parabolic orbit around the MBH, the ejection probability is equal between the two stars in the binary, independent on mass ratio (Sari et al. 2009a; Kobayashi et al. 2012). If we consider the isolated system of the MBH and the stellar binary, the velocity of the ejected star at infinity is

$$v = \alpha \sqrt{\frac{2Gm_{\rm cap}}{a_{\rm b}}} \left(\frac{M_{\rm MBH}}{m_{\rm b}} \right)^{1/6}, \tag{1.2}$$

where α is a prefactor of order unity, G the gravitational constant, and $m_{\rm cap}$ the mass of the captured companion (e.g. Rossi et al. 2014). The prefactor α depends on the exact geometry of the encounter including the phase of the binary, orbital inclination, eccentricity, and diving factor, where the diving factor is defined as the tidal separation radius over the pericentre of the centre-of-mass orbit (Sersante et al. 2025). Because the MBH is embedded in the Galaxy, the velocity defined above can be seen as the velocity at

which a star is ejected from the GC. For an equal mass binary, we can rewrite equation 1.2 to

$$v \simeq 1500 \text{ km s}^{-1} \left(\frac{m_\text{b}}{2M_\odot}\right)^{1/3} \left(\frac{a_\text{b}}{0.1 \text{ AU}}\right)^{-1/2} \left(\frac{M_\text{MBH}}{4.3 \times 10^6 \ M_\odot}\right)^{1/6} \alpha, \quad (1.3)$$

which clearly demonstrates the extreme velocities that the Hills mechanism can eject stars at. The captured star on the other hand is captured into an orbit around the MBH with a semi-major axis

$$a_\text{cap} = \frac{a_\text{b} M_\text{MBH}}{2\alpha^2 m_\text{ej}} \left(\frac{m_\text{b}}{M_\text{MBH}}\right)^{1/3}, \quad (1.4)$$

with m_ej the mass of the ejected star. Similarly to above, we can rewrite this as

$$a_\text{cap} \simeq 0.005 \text{ pc } \left(\frac{a_\text{b}}{0.1 \text{ AU}}\right) \left(\frac{m_\text{b}}{2 \ M_\odot}\right)^{-2/3} \left(\frac{M_\text{MBH}}{4.3 \times 10^6 \ M_\odot}\right)^{2/3} \frac{1}{\alpha^2}, \quad (1.5)$$

which shows that the captured stars can end up on orbits similar to the S-stars in the GC (see Section 1.1.4).

1.2.3 Alternative ejection mechanisms

We have discussed the Hills mechanism as an origin of HVSs, however there are alternative methods to accelerate stars to the escape velocity of the Galaxy. Here we will briefly discuss a number of these mechanisms. Before we do so, we should recognise that extragalactic HVSs should exist according to the same mechanisms as Galactic HVSs and that some might have already been discovered (Edelmann et al. 2005; Gualandris & Portegies Zwart 2007; Przybilla et al. 2008a; Evans & Massey 2015; Han et al. 2025). Similarly, the Hills mechanism can also operate with intermediate mass black holes in star clusters (Häberle et al. 2024).

As mentioned before, Yu & Tremaine (2003) identify two additional ejection mechanisms from the GC: gravitational encounters of single stars and ejections by a BBH. An ejection by a gravitational encounter between single stars is limited by the escape velocity from the surface of the star. This means that ejection velocities tend to be significantly lower compared to the Hills mechanism. Only for rare, close encounters can this mechanism eject a star with sufficient energy to escape from the Galactic bulge. The rate of these ejections is estimated to be orders of magnitude lower compared to the Hills mechanism with only $\sim 10^{-9}$ yr^{-1} able to reach out to the solar circle. For ejections involving a massive BBH, the average ejection speed is

$$v_\text{ej} \simeq \left(2.7 \times 10^3 \text{ km s}^{-1}\right) \left(\frac{\nu}{0.1}\right)^{1/2} \left(\frac{M_1}{4.3 \times 10^6 \ M_\odot}\right)^{1/2} \left(\frac{1 \text{ mpc}}{a_\text{BH}}\right)^{1/2}, \quad (1.6)$$

with ν the mass ratio between the less massive black hole and the BBH, M_1 the mass of the more massive black hole, and $a_{\rm BH}$ the semi-major axis of the BBH (Yu & Tremaine 2003). This ejection velocity is similar to the Hills mechanism, but requires an, as of yet, undetected companion to Sgr A* (e.g. Gualandris & Merritt 2009; Naoz et al. 2020; GRAVITY Collaboration et al. 2020; Evans et al. 2023). As opposed to the Hills mechanism, the BBH slingshot mechanism thus requires additional assumptions and it is not clear if this mechanism currently operates at the GC.

Neither of the alternatives to the Hills mechanism suggested in Yu & Tremaine (2003) thus provide an appealing explanation for currently observed HVSs travelling with velocities in excess of the escape velocity of the Galaxy. For completeness we also point out two more mechanisms that have been suggested in the literature: a variety of the first mechanism of Yu & Tremaine (2003), where stars are scattered of stellar mass black holes in the GC rather than other stars (O'Leary & Loeb 2008) and the disruption of a dwarf galaxy near the GC (Abadi et al. 2009). These two mechanisms both predict distinct properties of the ejected stars in comparison to the Hills mechanism and neither can convincingly explain the existence of S5-HVS1. The Hills mechanism is therefore the leading theory for the ejection of the currently observed HVSs. However, stars have been found in the stellar halo that are unbound to the Galaxy, but do not originate in the GC (e.g. Irrgang et al. 2018; Kreuzer et al. 2020; Irrgang et al. 2021). Note that according to our definition of HVSs—having been ejected from the vicinity of Sgr A*—these stars do not classify as HVSs. In the literature, often no distinction is made on the origin of the stars, with 'high velocity' sometimes being the only defining feature. Since such stars can easily be confused with HVSs, we discuss the two leading ejection mechanisms. Because these stars did not originate in the deep potential well of the GC, their ejection velocities can be lower while still being energetic enough to escape from the Galaxy.

The first mechanism to accelerate stars to velocities in excess of the escape velocity of the Galaxy is through core-collapse supernovae in binary systems (Blaauw 1961; Tauris & Takens 1998; Portegies Zwart 2000; Przybilla et al. 2008b; Evans et al. 2020). The rapid mass loss of the companion during the supernova in combination with a kick induced by an asymmetric explosion can accelerate the companion to velocities in excess of the escape velocity (e.g. Tauris 2015). Typical ejection velocities through this mechanism are, however, thought to be much lower at up to a few tens of $\mathrm{km\,s^{-1}}$ (e.g. Renzo et al. 2019). An alternative way to eject stars is through dynamical interactions in dense stellar systems (Poveda et al. 1967; Leonard & Duncan 1988, 1990; Leonard 1991; Perets & Šubr 2012; Oh & Kroupa 2016; Evans et al. 2025). The ejection velocity in this scenario is maximised for an encounter in which a physical collision is narrowly avoided, which limits the ejection velocity to below the escape velocity from the stellar surface (on

the order $\sim 600\ \mathrm{km\,s^{-1}}$ for a Sun-like star). The rates at which these two mechanisms produce ejections in excess of the escape velocity are thought to be significantly lower compared to the ejection rate from the GC, but remain highly uncertain (e.g. Silva & Napiwotzki 2011; Brown 2015; Evans et al. 2020; Irrgang et al. 2021; Evans et al. 2025).

1.2.4 HVS science cases

Now that we have established what HVSs are and how they can be formed, we go into the potential science cases. The science case that we attempt to exploit most throughout this work is the ability of HVSs to inform us about properties of the GC. The GC is a highly challenging region to study due to the relatively large distance (~ 8 kpc), high extinction ($A_\mathrm{V} \sim 50$; Fritz et al. 2011), and difficulty of resolving individual stars due to source crowding. However, this is also a very interesting region, since it is host to the MBH Sgr A*, the densest stellar environment in the Galaxy, and a plethora of stellar and dynamical phenomena that are not yet understood (for a review, see Genzel et al. 2010). HVSs offer a unique probe into this region of the Galaxy, because they are ejected out of the GC and are currently observable in the stellar halo, with little extinction and without the issue of source crowding. If these stars are ejected through the Hills mechanism, we know they were formed in a binary, likely near the GC (e.g. Penoyre et al. 2025). Their properties, such as metallicity, mass, and age are therefore informative for the same properties of stars near the GC, which is what some of the work in this thesis focusses on (Verberne et al. 2024a, 2025). These properties are extremely difficult to currently measure for stars near Sgr A* (e.g. Habibi et al. 2017b), while they are informative on the assembly history of the GC, star formation in extreme environments, and the evolution of Sgr A*. In addition, their velocity distribution is a measure of the progenitor binary semi-major axis and mass ratio distributions (Evans et al. 2022a), which are uncertain even for field stars (Moe & Di Stefano 2017). Furthermore, their distribution on sky can be used to infer if progenitor binaries approach the MBH isotropically and even if Sgr A* has (or had) a massive companion black hole (e.g. Evans et al. 2023, see also Section 1.2.3).

Another potential of HVSs is to measure the Galactic potential. Because we know the origin of these stars (the GC), their current position and velocity describe the Galactic potential (Gnedin et al. 2005; Yu & Madau 2007; Kenyon et al. 2008; Perets et al. 2009a; Rossi et al. 2017; Fragione & Loeb 2017; Kenyon et al. 2018; Contigiani et al. 2019; Gallo et al. 2022; Armstrong et al. 2025). Using HVSs to measure the Galactic potential has, however, proved challenging. The HVSs that are most sensitive to the Galactic potential are the ones that are ejected with a velocity similar to the escape velocity of the Galaxy (Rossi et al. 2014). The problem here arises because

these HVSs are typically also the most difficult to unambiguously associate with a GC ejection due their overlap in parameter space with other stellar populations (e.g. Przybilla et al. 2008b,a; Kreuzer et al. 2020; Irrgang et al. 2021). Meanwhile, the single unambiguous HVS (largely unambiguous due to its extreme velocity) is too fast to have been significantly affected by the Galactic potential (Koposov et al. 2020). Another challenge for measuring the Galactic potential using HVSs is that the number of observed HVSs required for these methods to be competitive is typically much larger than is currently observed.

A science case which has already proved successful is measuring the Solar motion and distance to the GC using HVSs, in particular S5-HVS1 (Hattori et al. 2018; Koposov et al. 2020). With a second HVS added to the analysis, the precision of this measurement will likely be comparable to that presented in GRAVITY Collaboration et al. (2019) (Koposov et al. 2020).

1.3 Large observational surveys

Critical for our understanding of the Galaxy and HVSs are the large observational surveys that have allowed us to study the stars around us in unprecedented detail. In order to determine the orbit of a star, we need to measure the radial velocity, the angular velocity and position in the plane of the sky, and the distance to the star. Especially over the past decades, various surveys have made significant strides in each of these areas (e.g. Perryman et al. 1997; York et al. 2000; Zhao et al. 2012; De Silva et al. 2015; Gaia Collaboration et al. 2016; Majewski et al. 2017a). Here we will discuss the two most important surveys for this thesis.

1.3.1 *Gaia*

Most prominent among the recent large surveys is the *Gaia* mission (Gaia Collaboration et al. 2016), which was a space-based observatory that had the ambitious goal of measuring astrometry for more than one billion stars. Astrometry deals with measuring the position and movement of stars and can be used to determine distances to stars and their velocities perpendicular to our line of sight. A full astrometric solution includes sky position, proper motion, and parallax. The proper motion of a star is its angular velocity in the plane of the sky, measured in two directions, with respect to a stationary reference frame of quasars. The parallax is the apparent movement of the position of a star by the change in viewing angle caused by observing a star at multiple points throughout the orbit of the telescope around the Sun. In Fig. 1.8, we schematically show the position of a star as a function of time under the effect of proper motion and parallax. The parallax of a star can

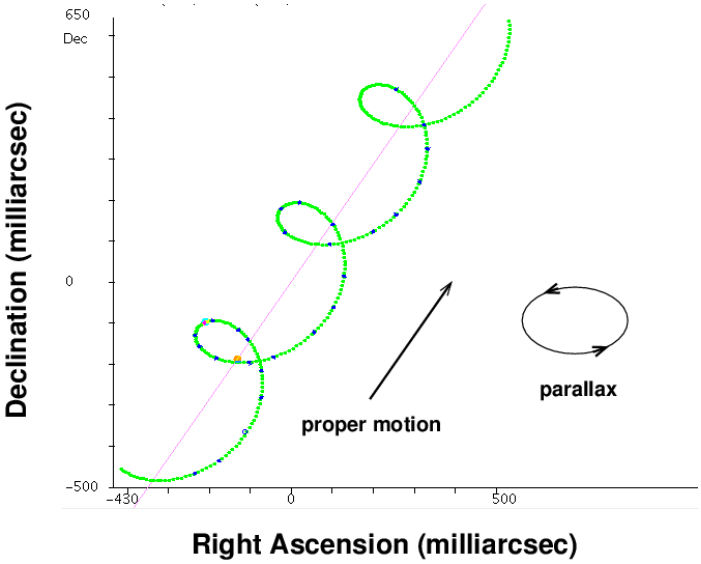

Figure 1.8: The on-sky movement of a star, which is the super position of the effects of proper motion and parallax. *Image credit: Michael Richmond.*

be used to determine the distance following

$$d = \frac{1}{\varpi}, \tag{1.7}$$

where d is the distance in kpc and ϖ the parallax in mas. *Gaia* works in an ingenious way to obtain these measurements. Unlike most telescopes, *Gaia* looks in two directions at the same time using two mirrors with fields-of-view separated by 106.5 degrees. The entire spacecraft spins at a fixed rate of 60 arcseconds per second around its spin axis. This rate has to be maintained precisely, since it is matched to the speed at which electrons are transferred inside the CCD. This also means that *Gaia* does not take pictures of the sky in the way we are familiar with for most other optical telescopes. The spin axis is such that one of the telescopes 'leads' while the other 'follows', making the two fields of view pass the same parts of the sky. The spin axis itself is inclined by 45 degrees with respect to the Sun to allow optimal parallax sensitivity. Finally, *Gaia* also precesses with a period of 63 days to allow it to observe the entire sky. The way that *Gaia* effectively observes the sky is called the scanning law, since the way *Gaia* observes is akin to scanning. Light from both fields of view ends up at the focal plane of *Gaia* shown in Fig. 1.9. The blocks correspond to individual CCDs, while their colours show the different functions. On the left we see the Sky Mapper CCDs, which handle object detection. In the middle are the Astrometric

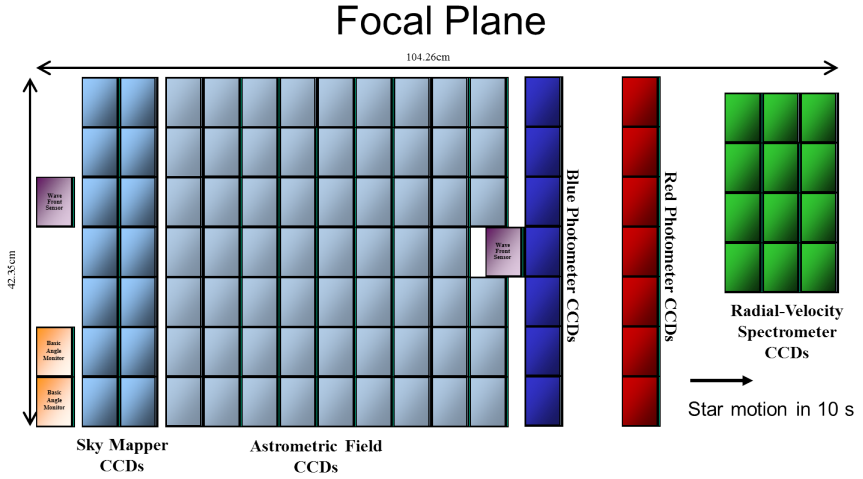

Figure 1.9: Focal plane of *Gaia* showing the different types of CCDs and their layout. *Image credit: ESA. Acknowledgement: Alex Short.*

Field CCDs, which perform the astrometric measurements. Next to that, we see in blue and red the Photometer CCDs, which provide low-resolution spectro-photometric measurements. Finally there are the Radial-velocity Spectrometer (RVS; Cropper et al. 2018) CCDs, which take high resolution spectra of bright sources. We will now discuss the main data products that these instruments provide.

The latest *Gaia* data release at the time of writing is data release 3 (DR3; Gaia Collaboration et al. 2023a), which has provided full astrometric solutions to about 1.46×10^9 sources with a limiting magnitude of $G = 20.7$, including magnitudes in three broad-band filters: G, $G_{\rm BP}$, and $G_{\rm RP}$. For the brightest of these stars, some 34 million, radial velocity measurements are available from the RVS (Katz et al. 2023). Although this is the largest precision radial velocity catalogue available, it only covers a fraction of the sources with full astrometric solutions in *Gaia*. New in *Gaia* DR3 compared to DR2 have been the low-resolution BP/RP spectra from the red and blue photometers (Gaia Collaboration et al. 2016; Montegriffo et al. 2023; De Angeli et al. 2023). Currently, these spectra are published for some 220 million sources, while with the next data release they will be published for all sources in *Gaia*. Although much lower resolution compared to the RVS spectra, the wavelength range covers the entire optical spectrum for sources with a limiting magnitude of $G = 17.65$. These low-resolution spectra are the subject of Chapter 2 of this thesis (Verberne et al. 2024b).

Now that we have gone over the main data products that the *Gaia* cata-

logue provides, we will discuss the limitation in using parallax measurements from *Gaia* to measure distance. For stars with $G < 15$, the median parallax uncertainty from *Gaia* data release 3 (DR3) is $0.02 - 0.03$ mas (Gaia Collaboration et al. 2023a). It should be clear that *Gaia* can therefore not effectively constrain distances beyond a few tens of kpc, given the inverse relation between distance and parallax. However, it turns out that obtaining a distance from simply inverting the parallax becomes problematic much sooner (Luri et al. 2018). While parallax can be negative, distance cannot. This, in combination with the non-linear relation between distance and parallax, causes the normally distributed uncertainties on the parallax to not translate into normally distributed uncertainties in distance space. It should also be noted that there are systematic biases present, such as the zero-point offset in the parallax (Lindegren et al. 2018, 2021). Bailer-Jones (2015) argue that once the relative uncertainty on the parallax exceeds 20%, it becomes non-trivial to obtain an unbiased distance estimate. Simple distance estimates from inverting the parallax can therefore typically only be used up to at most a few kpc with the data from *Gaia*. Beyond these distances, additional information should be incorporated when considering the distance, such as colour, magnitude, and sky position (Bailer-Jones et al. 2018, 2021).

Also, although the limiting magnitude of *Gaia* is $G = 20.7$ as mentioned before, that does not mean that every source brighter than this limit is represented in the *Gaia* catalogue. If we imagine a fictitious star with properties $\vec{p}$ located at different positions in the sky, the chance of this star appearing in the *Gaia* catalogue is not fixed. For various reasons including a limit on the number of sources that *Gaia* can detect simultaneously, source crowding in some parts of the sky, and uneven sky coverage due to the scanning law, *Gaia* is more 'complete' in some directions than others. We show the chance of a star with $G = 21$ appearing in the *Gaia* DR3 catalogue in Fig. 1.10. In the figure we can recognise some of the dependencies mentioned above. Most obvious is the pattern of stripes, which is caused by the scanning law: the red areas tend to be observed more often. In addition, we see that the GC, at the centre of the figure, has a low completeness at $G = 21$, which is caused by the large number of sources saturating *Gaia*. The chance for a star with properties $\vec{p}$ to be observed at various positions in the sky is referred to as the selection function. Note that $\vec{p}$ are the properties as seen from the observer, which means that interstellar extinction does not directly influence the selection function. In the case of *Gaia*, the selection function is fairly well defined thanks to the efforts of the GaiaUnlimited team (Cantat-Gaudin et al. 2023; Castro-Ginard et al. 2023) and can be mostly characterised by sky position and G magnitude.

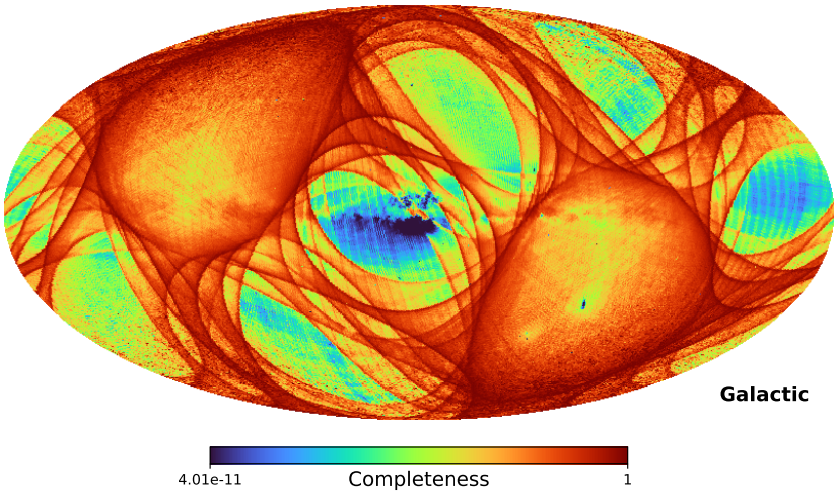

Figure 1.10: The completeness of the *Gaia* catalogue at $G = 21$ as a function of sky position in Galactic coordinates.

1.3.2 DESI

The Dark Energy Spectroscopic Instrument (DESI; DESI Collaboration et al. 2016a) is a multi-object spectrograph located at Kitt Peak National Observatory in Arizona, capable of taking 5000 spectra simultaneously (DESI Collaboration et al. 2016b). The instrument is designed to study cosmology, but also observes stars as secondary targets as part of its Milky Way Survey (MWS; Cooper et al. 2023; Koposov et al. 2025). Despite stars being a secondary target, the MWS survey is still expected to observe more than 12 million stars in total (Koposov et al. 2025). The wavelength coverage of DESI is $360 - 980$ nm spread over three channels, which covers the entire visible wavelength range and part of the near-infrared. The spectral resolution $R = \lambda/\Delta\lambda$ over this range varies between 2000 and 5000. *Gaia* RVS in comparison has a higher resolution at $R = 11\,500$, but only a very narrow wavelength range $\lambda \in [845, 872]$ nm. Another key difference between DESI and *Gaia* RVS is the magnitude range covered, which we show in Fig. 1.11. We can see that *Gaia* RVS is overall the largest catalogue, but only covers relatively bright stars. DESI on the other hand is the largest catalogue for faint sources with $17 \lesssim G \lesssim 21$. In addition to above mentioned characteristics, a key difference of DESI compared to *Gaia* is that DESI only covers part of the sky, which is a consequence of both survey strategy and the limitation of being a ground based observatory.

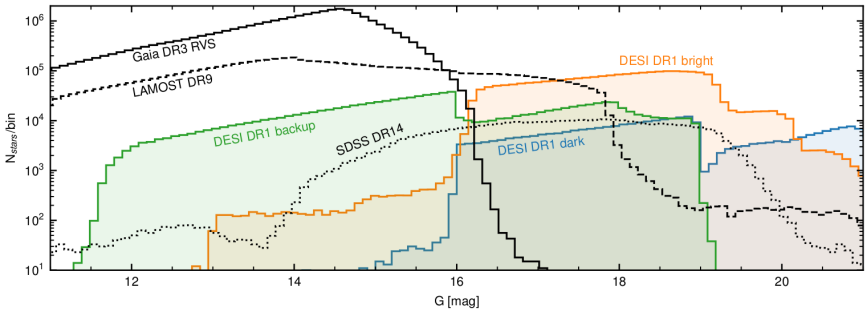

Figure 1.11: The number of stars with spectroscopic (radial velocity) measurements as a function of G magnitude in various surveys. Note that DESI DR1 is currently the largest catalogue for stars with $17 \lesssim G \lesssim 21$. *Figure from Koposov et al. (2025).*

In the final chapter of this thesis, we will use DESI DR1 (DESI Collaboration et al. 2025a), which was released in March 2025. This data release includes spectra and data products for $\sim$ 2.5 million stars as part of the bright program, which is the main program for the MWS (Koposov et al. 2025) and the program we use in Chapter 5. Apart from radial velocities, the value-added catalogues of DESI DR1 also contain measurements of distance, metallicity, α enhancement, and a number of individual elements.

1.4 Future observational prospects

Now that we have gone over the background for this thesis, we will discuss the future prospects for HVSs, where we focus on the observational aspect.

Science exploitation of HVSs has so far been limited by the number of known HVSs. Identifying additional HVSs is therefore of prime importance in the field. The most exciting prospects for identifying more HVSs are the ongoing and upcoming large spectroscopic surveys by *Gaia* (including astrometry), *WEAVE* (Dalton et al. 2014; Jin et al. 2024), DESI, and *4MOST* (de Jong et al. 2019).

Although *Gaia* has recently been decommissioned, a wealth of data remains unpublished and will be released in DR4 and DR5. The latest DR3 only publishes data from the first 34 months of *Gaia* operations between 2014 and 2017. Meanwhile *Gaia* continued to observe till it was decommissioned in early 2025 (Gaia Collaboration et al. 2021). In DR4, *Gaia* will publish radial velocities for more than 100 million stars, in addition to individual epoch measurements (Katz et al. 2023). The large increase in radial velocities in combination with improved accuracy and precision for the astrometric measurements is expected to allow for much more sensitive

HVS searches (e.g. Evans et al. 2022a,b).

Despite *Gaia* increasing the number of stars with measured radial velocities by a factor of at least a few in the next data release, these measurements will still be limited to the relatively bright stars with $G_{\rm RVS} \lesssim 16$. The aforementioned large ongoing and upcoming spectroscopic surveys performed by DESI, *WEAVE*, and *4MOST* will provide millions of radial velocity measurements for stars up to *Gaia*'s limiting magnitude of $G = 21$. In addition, these instruments, unlike *Gaia*, also allow for targeted follow-up observations of promising HVS candidates. These HVS candidates can be identified using available data, such as distance, colour, brightness, and astrometry. Spectroscopic follow-up observations can then be used to measure the radial velocities to these stars, which might allow confirmation or rejection of the HVS candidates. This method is much more efficient compared to magnitude limited radial velocity surveys such as *Gaia* in identifying HVSs. The multi-object spectrographs on the aforementioned instruments allow the simultaneous measurement of a thousand or more radial velocities. This means that follow-up observations of large numbers of HVS candidates become feasible. For instance about 20 000 HVS candidates will be observed as part of the high-latitude low-resolution survey of *WEAVE*. This is in addition to the possibility of serendipitous HVS discoveries in these surveys of course.

Apart from larger surveys, more effective identification of HVS candidates is an area with a lot of potential for improvement. For instance, the first HVS survey only relied on colour-magnitude information to identify HVS candidates. More recently, many 'blind' searches have been conducted for HVSs, in which all stars with 6D phase-space information are analysed to search for stars with either high Galactocentric velocities and/or a trajectory that is consistent with originating in the GC. However, the astrometric data provided by *Gaia* also facilitates more sophisticated selection procedures, such as presented in Chapter 3. The challenge in identifying HVS candidates often comes down to a trade-off between completeness and purity. Completeness refers to the fraction of true HVSs that a method will identify, while purity refers to the ratio of true HVSs over the total number of identified candidates. Applying more stringent requirements to consider a particular star to be an HVS candidate will typically decrease the completeness, while improving the purity.

1.5 Thesis content

In this thesis we use state-of-the-art observations and simulations to provide the best constraints to date on the HVS ejection rate and constraints on the stellar content and dynamics at the GC, including the progenitor binary populations and their star formation history. The challenge in identifying

HVSs is often the observational volume of the sample that is used, which is a common thread through most of the chapters in this thesis. We first attempt to identify new HVSs by increasing the number of stars with radial velocity solutions using the 220 million low resolution spectra provided by *Gaia* DR3, before switching to a method that looks for the fastest ($> 800\,\mathrm{km\,s^{-1}}$) HVSs in all ~ 1.5 billion sources in *Gaia*. In Chapter 4 we combine these measurements with observations of the GC to perform a robust analysis linking the S-stars with the stars captured by the Hills mechanism and in the final chapter we use the newly released DESI DR1 MWS to further increase our observational footprint and search instead for HVSs ejected over billions of years that have remained bound to the Galaxy. We briefly summarise each chapter below.

In Chapter 2 we start out by attempting to measure radial velocities from the aforementioned *Gaia* BP/RP spectra in *Gaia* DR3. Our goal is to increase the number of sources with 3D velocities, since that makes it more straightforward to identify HVS candidates. Using model grids of stellar spectra, we fit every available BP/RP spectrum and marginalise over all stellar parameters other than radial velocity. We find that BP/RP spectra in *Gaia* can be used to measure radial velocities, albeit at much lower precision compared to, for instance, *Gaia* RVS. We perform calibration of the radial velocities in colour-magnitude-extinction space and publish a catalogue of BP/RP measured radial velocities. Our extended catalogue, containing some 125M radial velocity measurements is to our knowledge the largest radial velocity catalogue to date. Despite the size of our catalogue, we find that identifying HVSs from our catalogue is non-trivial, due to the large nominal uncertainties and a fraction of sources with unreliable measurements.

In Chapter 3 we follow a different approach to identify HVS candidates. Instead of only looking at stars with 3D velocity measurements, we use a novel method to select stars that appear to be travel on radial trajectories from the GC, which can be applied to all ~ 1.5 billion stars with astrometric solutions in *Gaia*. We create a catalogue of 600 HVS candidates, based on their proper motions, sky position, and colour and perform follow-up observations for about 200 of those using ground-based spectroscopic instruments. Because we use both northern and southern hemisphere telescopes, we can cover our HVS candidates across the sky. We use the non-detection of new HVSs among our 200 observed HVS candidates in combination with sophisticated simulations to significantly improve constraints on the ejection rate and mass function of HVSs and provide predictions for the undiscovered population of HVSs in *Gaia*.

Chapter 4 in a way is the odd one out in this thesis, since we do not attempt to discover new HVSs. Instead we combine observations of the GC with our own observational catalogue described in Chapter 3 and compare to simulations to investigate if the Hills mechanism alone can explain the

observed properties of the S-star cluster. We use realistic star formation histories for stars near the GC and simulate binary disruptions. We find that no single progenitor binary population can explain all the observed properties of both the S-star cluster and HVSs simultaneously. Instead, we find that at least two progenitor populations are required: an old population and a young population. Assuming that the young population is the CWD near Sgr A* and the old population undergoes Hills mechanism disruptions at a constant rate, we find that the recent star formation episode at the GC which formed the CWD has boosted the Hills mechanism disruption rate by about an order of magnitude compared to the background rate over the past ~ 10 Myr.

Finally in Chapter 5 we again aim to identify new HVSs by going to an even larger potential discovery space: stars ejected from the GC that have remained bound to the Galaxy. Since HVS ejections will have been happening for billions of years and a significant fraction of these is expected to remain bound to the Galaxy, a population of stars ejected from the GC should have accumulated in the stellar halo. Using the recently released DESI DR1 MWS survey data, we aim to statistically identify an overdensity of high metallicity stars on low angular momentum orbits, characteristic of stars ejected from the GC. Although we obtain a null-detection for a GC ejected population of stars, we use this null-detection to put upper limits on the ejection rate of stars from the GC over the past ~ 5 Gyr, which is ejection model independent.